Remote Sensing of Environment 152 (2014) 638–653

Contents lists available at ScienceDirect

Remote Sensing of Environment

journal homepage: www.elsevier.com/locate/rse

Using land surface microwave emissivities to isolate the signature of snow on different surface types

Narges Shahroudi [1], William Rossow [2]

CREST at The City College of New York, Steinman Hall, 140th Street and Convent Avenue, New York, NY 10031, USA

ARTICLE INFO

Article history:
Received 3 December 2013
Received in revised form 2 July 2014
Accepted 3 July 2014
Available online xxxx

Keywords:
Microwave remote sensing
Snow
Emissivity

ABSTRACT

The objective of this paper is to better isolate the snow signature in microwave signals to be able to explore the ability of satellite microwave measurements to determine snowpack properties. The surface microwave effective emissivities used in this study are derived from SSM/I passive microwave observations by removing the contributions of the cloud and atmosphere and then separating out the surface temperature variations using ancillary atmospheric, cloud and surface data. The sensitivity of the effective emissivity to the presence/absence of snow is evaluated for the Northern Hemisphere. The effect of the presence of snow, the variation of land types, and temperature on the emissivities have been examined by observing the temporal and spatial variability of these measurements between 19 and 85 GHz over the Northern Hemisphere. The time-anomaly of differences between effective emissivity at 19 V and 85 V enabled the constant effects of land surface vegetation properties to be removed to isolate the snow signature. The resulting 12-year snow signal combined with skin temperature data can detect the existence of snow cover over the Northern Hemisphere on daily basis. The results of this method compared with the operational NOAA weekly snow cover maps agree at 90% of locations and times. Most of the disagreements could be explained by rapid evolution of snow emissivities associated with freeze–melt–refreeze cycles and precipitation (snowfall), and some of them by the space–time resolution differences of the microwave and operational snow cover determinations. These results compared with the NISE, NOAA IMS, CMC, and MODIS, and snow products agree within 78% to 92%.

1. Introduction

Seasonal snow typically covers 30% of the total land area of the Northern hemisphere. Snow cover is a significant climate indicator and an important factor controlling the amount of solar radiation absorbed by earth. Snowmelt resulting from a warming trend would increase the absorption of solar radiation, a positive feedback. Moreover, snow plays a different role than liquid water in the processes affecting surface evaporation (latent heat), soil moisture supply to vegetation and runoff. Snow acts as a temporary reservoir of water that is crucial to water supply in many regions (Robinson, Dewey, & Heim, 1993). Because of the complex interaction of snow with the landscape and varying atmospheric conditions, monitoring the spatial and temporal variability of snow properties at relatively high space–time resolution provides valuable information on surface hydrology and radiation.

The use of satellite remote sensing for mapping snow cover and measuring snow characteristics has a long history reaching back to the 1960s. Dietz, Kuenzer, Gessner, and Dech (2012) reviewed all the available methods of measuring snow using satellite data and looked at each method's advantages and disadvantages. For example, passive microwave radiances from satellites overcome the main limitations of visible measurements by being able to sense the surface at night and through non-precipitating clouds, improving time resolution to near daily. Although spatial resolution is poorer and the sensitivity to small amounts of snow is less than for visible radiation measurements, the microwave signal is also sensitive to other snow properties such as density, depth, and crystal-size distribution. However, this sensitivity is confounded by sensitivity to the variations of other land surface properties such as temperature, surface wetness, melting–refreezing cycles, and embedded or covering vegetation.

The main objective of this paper is to better isolate the snow signature in microwave signals to explore the ability of satellite microwave measurements to determine other properties of snowpack besides cover extent. The microwave signal acquired from the satellite is the combination of the land surface and atmospheric contributions. The microwave emission of the land surface itself is the product of its physical temperature and the surface emissivity (this product is the brightness temperature). The surface emissivity represents the intrinsic physical characteristics of the land surface and is sensitive to variations

E-mail addresses: nshahro00@citymail.cuny.edu (N. Shahroudi), wbrossow@ccny.cuny.edu (W. Rossow).
[1] Tel.: +1 212 650 7000x13795.
[2] Tel.: +1 212 650 5389.

http://dx.doi.org/10.1016/j.rse.2014.07.008
0034-4257/

of vegetation density, soil moisture, surface composition, and standing water at the surface as well as snow properties. Thus, to isolate the changes in satellite microwave measurements associated with snow, we need to account for all the other contributions to the signal to develop generally valid, global measurement of snow properties such as snow depth, snow grain size, and snow water equivalent.

There are number of studies using passive microwave satellite observation over snow to estimate snow properties (Chang, Foster, & Hall, 1987; Foster et al., 1996; Grody & Basist, 1996; Hall et al., 1991; Kelly & Chang, 2003; Kunzi, Patil, & Rott, 1982), but most of these studies analyze microwave brightness temperatures alone. Brightness temperature variation is strongly affected by the variation of the surface physical temperature as well as changes in other land surface properties. Although using differences of brightness temperatures at different frequencies substantially reduces the surface temperature dependencies, global applications of such results have been questioned because of the complex signature of snow on varying landscapes as well as the relatively low spatial resolution of passive microwave measurements. Many liquid water clouds produce changes in microwave brightness temperatures similar in magnitude to that of water vapor [Lin & Rossow, 1994].

In this study we use land surface emissivities retrieved from the passive microwave brightness temperature (Aires, Prigent, Rossow, & Rothstein, 2001, see Section 2 data), by removing the contributions of cloud and atmosphere and separating surface temperature. The remaining variability in the emissivities is due to changes of the land surface characteristics (soil moisture, vegetation density, surface wetness) as well as the snow properties. To investigate removal of the other non-snow surface effects from the signal, we examined the space–time variability of land emissivities for different vegetation categories with and without the presence of snow. The effect of land is removed from the signal (approximately) by subtracting the mean snow-free emissivity of each location from its emissivity with snow present. The operational NOAA snow cover charts, providing weekly snow cover from satellite visible image analysis, are used for snow/snow free separation in this part of the analysis. When all the contributions to the signal except snow have been removed, the remaining variability of the snow signal is examined over time for each location. Infrared skin temperatures (Prigent, Aires, & Rossow, 2003a,b) and the reference snow cover (see Section 2) data are used to find an emissivity-dependent threshold that distinguishes between snow/snow free land from the microwave emissivities.

The satellite observations and the ancillary datasets used in this study are described in Section 2. In Section 3, the steps to isolate the snow signal are described. Also in this section we emphasize the spatial and temporal variability of the emissivities over snow-covered regions to characterize their fluctuations with vegetation, temperature and precipitation. In Section 4 a global snow cover identification technique is proposed and is compared with the operational NOAA snow cover charts. As a test of sensitivity the specific cases for which our results and the operational snow charts do not agree are examined to see if these disagreements can be explained. Section 5 compares the results of our snow cover detection with the newer daily NOAA IMS snow flag, the Canadian Meteorological Center (CMC) snow depth station data, the MODIS snow cover product, and the Near-Real-Time Ice and Snow Extent (NISE) from microwave. Section 6 examines the variation of snow cover over the whole 12-year record and compares some interesting features with results from other available snow cover products. Section 7 concludes this study.

2. Data

2.1. Land microwave emissivity (EM) & skin temperature (TS)

The SSM/I instruments on board the Defense Meteorological Satellite Program (DMSP) polar orbiters observe the Earth twice daily (typically near dawn and dusk) with observing incident angle close to 53° for flat a surface and a field-of-view decreasing with frequency from 43 km × 69 km at 19 GHz to 13 km × 15 km at 85 GHz (Hollinger, Lo, Poe, Savage, & Pierce, 1987). The SSM/I channels measure brightness temperatures (TB) at 19.3 GHz, 22.2 GHz, 37.0 GHz and 85.5 GHz at vertical and horizontal polarizations except at 22 GHz, which is only in vertical. SSM/I was the first passive microwave satellite that had external calibration by viewing a mirror that reflects cold space and a hot reference target once each scan, every 1.9 s (Gentemann, Wentz, Brewer, Hilburn, & Smith, 2010).

Prigent, Aires, Rossow, and Matthews (2001) and Prigent, Rossow, and Matthews (1997) determined land surface microwave emissivities from the SSM/I brightness temperatures by removing the effects of the atmosphere, clouds, and rain (Aires et al., 2001) using ancillary data from ISCCP (Rossow & Schiffer, 1999) and the NCEP reanalysis (Kalnay et al., 1996). First, the cloud-free SSM/I observations are isolated using collocated visible/infrared satellite observations from ISCCP. The cloud-free atmospheric contribution is then calculated from temperature–humidity profiles from the NCEP reanalysis. Finally, surface skin temperature (TS) is taken from ISCCP (corrected for the original assumption of unit IR emissivity in the ISCCP product using surface-type-dependent IR emissivities) to determine the surface emissivities for the seven SSM/I channels. The calculated emissivities can be related to the intrinsic surface properties independent of atmospheric contributions or the variations of TS. The true emissivity is defined by the normalization of TB by the effective soil temperature corresponding to the contributions of all the surface layers of the ground weighted by their attenuation (Wigneron, Chanzy, de Rosnay, Rudiger, & Calvet, 2008). Hence the emissivities used in this paper are "effective" values because they are derived from the normalization of TB by the skin temperature (TS). The spectral gradient of effective emissivities is an index that approximates the true spectral emissivity difference.

The effective emissivities are determined on an equal area grid equivalent to 0.25° × 0.25° at the equator and are compiled daily from 1992 to 2004 (recently extended through 2008). For illustration, monthly mean effective emissivities (EM) are shown in Fig. 1 for 19 V, 37 V, and 85 V GHz for December 2002. In this paper, we will use EM followed by numbers to indicate frequency and "H" or "V" to indicate polarization, for example, EM19V or EM85H. If no letter is given, it means that the statement applies to both polarizations. EM followed by numbers and letters representing two channels, for example EM19V-37V or EM19H-85H, will represent the difference of effective emissivities at two frequencies. We also consider temporal anomalies of effective emissivity differences as the difference between the instantaneous effective emissivity difference at a location and a time-averaged value at the same location; we represent such quantities by δEM followed by numbers and letters representing the two channels, for example δEM19V-37V or δEM19H–85H.

The skin temperature (TS) is the physical temperature of the Earth's surface (which can be closer to the canopy top for dense vegetation). The infrared surface brightness temperature (IR emissivity assumed to be unity) is determined at 3-hour intervals since 1983 over the globe every 30 km from a combination of polar and geostationary satellite (Rossow & Schiffer, 1999). Two values of TS are reported; one based on the IR clear sky radiances from the 5-day composites and one based on any available clear pixel IR radiances; the former values are a better estimate of TS because the latter values are slightly cloud contaminated by design (Rossow & Garder, 1993). The ISCCP TS values are corrected for non-unit emissivities using a land classification to specify IR emissivities (Zhang, Rossow, Lacis, Oinas, & Mishchenko, 2004). The corrected ISCCP TS values at 3-h intervals are interpolated to match the SSM/I over flight time and mapped to the same 25 km grid. For illustration, the monthly mean skin temperatures for December 2002 are presented in Fig. 1.

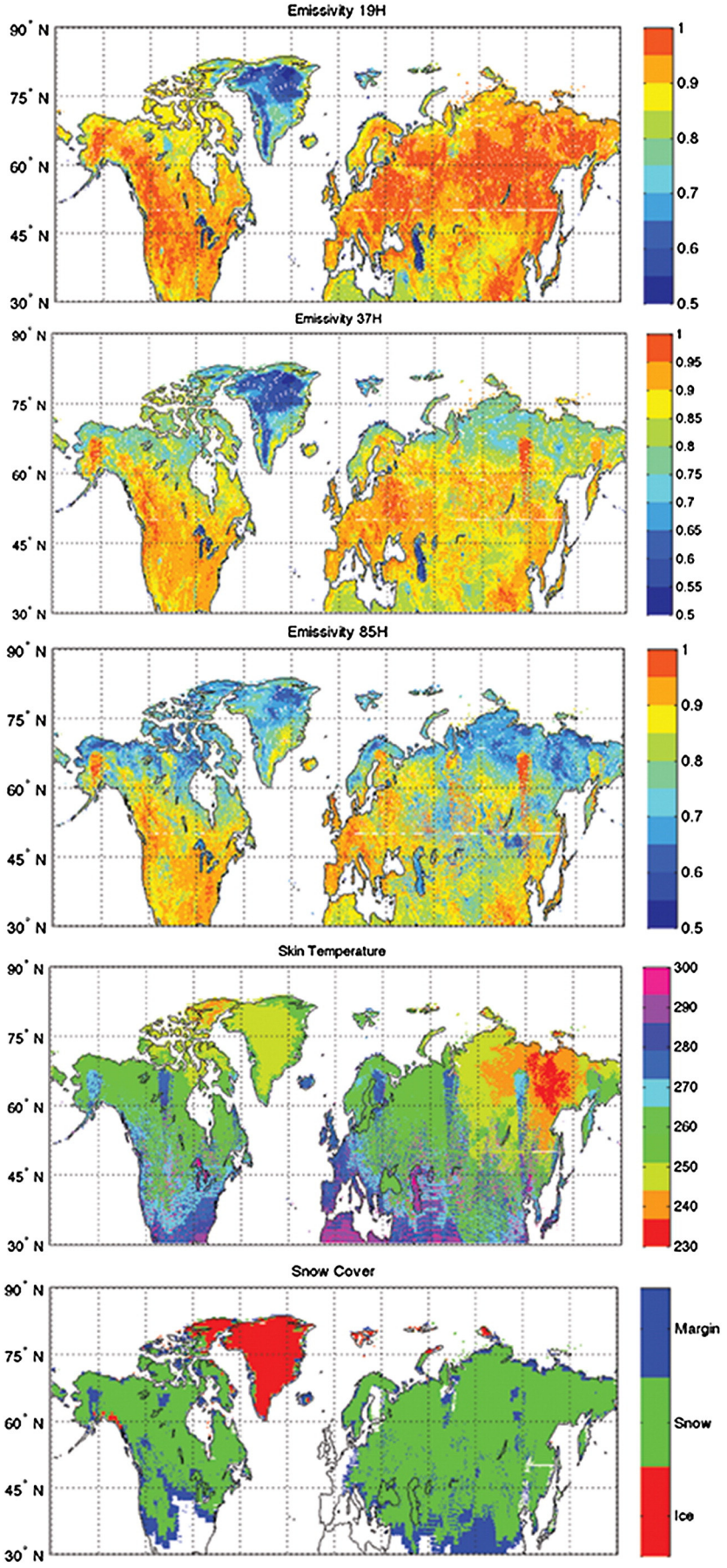

Fig. 1. Dec 2002 mean effective emissivity map for 3 channels (19H, 37H, 85H), with the corresponding mean skin temperature and snow cover map.

2.2. Snow cover

The NOAA Operational snow cover product is used to develop the microwave-based snow detection algorithm and another four products (IMS, CMC, MODIS, and NISE) are used to evaluate the final product. We focus on the Northern Hemisphere in this study.

2.2.1. NOAA Operational Weekly Snow Cover Charts (SC)

The operational Northern Hemisphere Weekly Snow and Ice Cover Charts, prepared by the Synoptic Analysis Branch at National Oceanic and Atmospheric Administration (NOAA) since 1966 (Dewey & Heim, 1982) are used in the ISCCP cloud analysis to indicate the presence of sea ice and snow in separating clear and cloudy scenes (Rossow & Garder, 1993). The ISCCP version of this information is available in a 1° equal-area grid at 5-day intervals (interpolated from the original 7-day NOAA product), where permanent ice cover locations in Greenland and Antarctica are also labeled as snow, but has been re-projected to the matched ISCCP and SSM/I pixels twice daily on a 25 km grid for convenience. This product also assumes snow cover for all regions in winter darkness. For illustration, the monthly mean snow cover for December 2002 is presented in Fig. 1. This visible-radiant-based snow cover product is used to develop the most sensitive microwave snow detection algorithm.

2.2.2. NOAA Interactive Multisensor Snow and Ice Mapping System (IMS)

The National Ice Center (NIC) of NOAA/NESDIS produces a daily snow and ice cover product for the Northern Hemisphere, Continental United States, Alaska, Afghanistan and Asia/Europe. The data are derived from several data sources, including the POES AVHRR and AMSU, GOES/Imager, GMS, and Meteosat. In 1997, the Interactive Multisensor Snow and Ice Mapping System (IMS) became operational, giving the satellite analysts improved access to imagery and drawing tools. Since the inception of IMS, the charts have been produced daily at nominal resolutions of 24 km and 4 km in a polar stereograph projection (NOAA/NESDIS/OSDPD/SSD, 2004). The 24 km version was used in this study since it better matches with our 25 km passive microwave dataset.

2.2.3. Canadian Meteorological Centre (CMC) snow depth

Canadian Meteorological Centre (CMC) compiles the Northern Hemisphere snow depth analysis data from surface synoptic observations (synops), meteorological aviation reports (metars), and special aviation reports (SAs) acquired from the World Meteorological Organization (WMO) information system for use in the CMC analyses. The CMC dataset includes daily observations from 1998 through 2010. The snow depth data are in polar stereographic projection with 24 km resolution (Brown & Brasnett, 2010).

2.2.4. Moderate Resolution Imaging Spectroradiometer (MODIS) snow cover

NSIDC archives and distributes snow cover and sea ice data products obtained from the Moderate Resolution Imaging Spectroradiometer (MODIS) sensor on NASA's Earth Observing System (EOS) Aqua and Terra satellites. The MODIS product contains snow cover, snow albedo, fractional snow cover, and Quality Assessment (QA). The data are gridded at 500 m intervals in a sinusoidal map projection over the whole globe. The results are reported daily at any location that is illuminated and cloud free; thus, over the wintertime due to the longer nights and cloudy sky, less than 50% of land is observed on a typical day. The snow cover determinations are based on a snow-mapping algorithm that employs a Normalized Difference Snow Index (NDSI) and other test criteria (Hall & Salomonson, 2006).

2.2.5. Near real time ice and snow extent (NISE)

The Near-Real-Time SSM/I-SSMIS EASE-Grid Daily Global Ice Concentration and Snow Extent product (Near-Real-Time Ice and Snow Extent, NISE) provides daily, global near-real-time maps of sea ice concentrations and snow extent. The National Snow and Ice Data Center (NSIDC) creates the current NISE product using passive microwave data from the Special Sensor Microwave Imager/Sounder (SSMIS) on board the Defense Meteorological Satellite Program (DMSP) F17 satellite. Snow extent is mapped separately using an algorithm developed for Scanning Multichannel Microwave Radiometer (SMMR) data where, snow depth $= 1.59 * (TB18H–TB37H)$ cm (Chang et al., 1987) and the algorithm was modified for use with SSM/I data as described in Armstrong and Brodzik (2001). NSIDC modified the snow extent mapping algorithm in March 2002, based primarily on a recent study by Armstrong and Brodzik (2002). The snow/ice maps are in EASE-Grid projection with 25 km resolution. This product is used to represent other snow cover products obtained by application of microwave brightness temperature algorithms (Nolin, Armstrong, & Maslanik, 1998).

2.3. Vegetation

A 1° spatial resolution land surface vegetation classification based on Matthews (1983) distinguishes a large number of vegetation types grouped into 9 classes: rain forest, deciduous forest, evergreen forest, shrubland, tundra, grassland and desert. Associated with the vegetation classification is a land use dataset that distinguishes five levels of cultivation intensity, ranging from 0 to 100% for 1° cells (Matthews, 1983). We focus on the five types of vegetation that experience seasonal snow cover: evergreen and deciduous forests, shrubland and grasslands, and tundra, which cover together about 80% of the whole Northern Hemisphere.

2.4. Precipitation

The Global Precipitation Climatology Project (GPCP) was established by the World Climate Research Program to quantify the distribution of precipitation around the globe over many years. Over land data from over 6000 rain gauge stations, and satellite geostationary and low-orbit infrared and passive microwave are merged to estimate rainfall from 1979 to the present. We use the GPCP-1DD version 6 product that reports precipitation at 1° and daily intervals (Adler et al., 2003; Huffman et al., 1997).

2.5. Space–time sampling of data

Each of the datasets described above has different intrinsic spatial and temporal resolutions. In order to compare all the snow datasets and the effective emissivity, skin temperature, vegetation, and precipitation data, all of these products were projected onto the same equal area, 25 km map grid at daily intervals. These conversions are done by the simplest procedure of reporting the nearest in space–time value from the original product in the target 25 km, daily version. Such a re-projection creates differences when comparing these datasets, so we have investigated the effects of changing space and time resolution using our 25 km, daily snow product to test how much the snow cover differs when compared to itself but in degraded resolution form. Spatial resolution was reduced in three different ways: averaging all the 0.25-degree pixels in a 1-degree grid to obtain a snow fraction, labeling a 1-degree grid as 100% snow if at least one 0.25 degree grid is labeled as snow and labeling a 1-degree grid as 100% snow if a majority of the 0.25-degree grids are labeled as snow. Comparing these 1-degree data with the original 0.25-degree data produces a disagreement frequency of about 3% (when comparing absence or presence). Temporal resolution was reduced from daily to weekly in similar fashion: averaging to obtain a snow fraction, labeling the week as 100% snow if any day in the week is labeled as snow, and labeling a week as 100% snow if the majority of days are snow covered. Comparing the new weekly data to the original daily data produces a disagreement frequency of

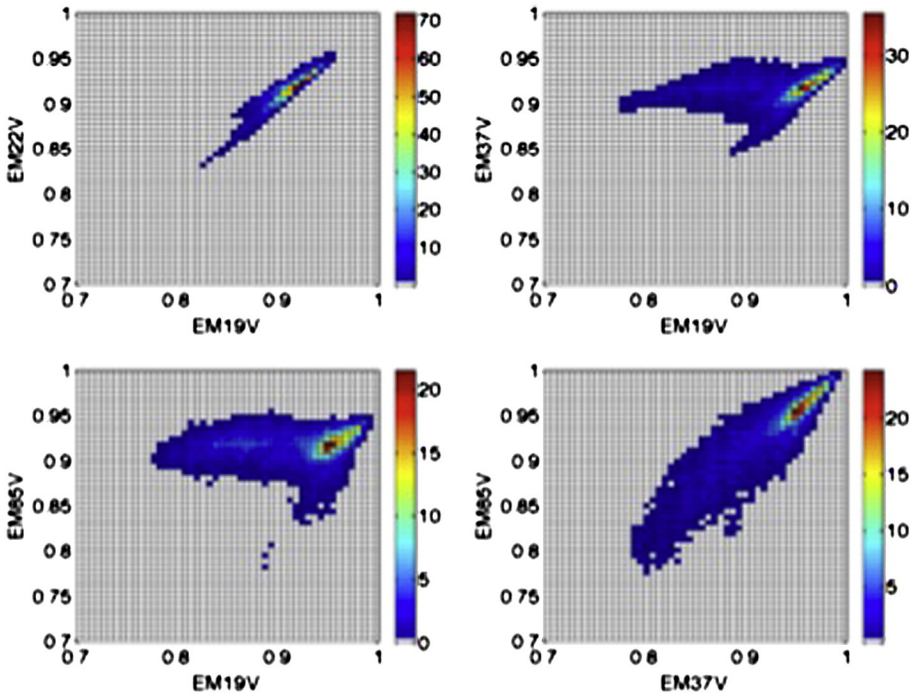

Fig. 2. Scatter plots of different channels of effective emissivity versus each other where the color bar shows the percentage of distribution of the point.

about 4%. These tests indicate that disagreement frequencies of at least 3%–4% can be produced by the mis-matched space and time resolutions of the products. That the sampling errors are so small also suggests that snow cover is fairly persistent in time and tends to cover large areas, producing most of the disagreement near the edge of the snow-covered region.

3. Variability of microwave emissivities

3.1. Frequency dependence

Land surface microwave effective emissivities over snow exhibit large spatial variability for a given month (Fig. 1). In December, for instance, the land north of 45° is fully covered by snow yet the effective emissivity values range between 0.6 and 1. The same fully snow covered area can have EM19H values between 0.9 and 1, between 0.8 and 1 for EM37H, and between 0.6 and 1 for EM85H. In general higher frequencies exhibit a larger range of land surface effective emissivities for snow-covered areas. The differences in EM range and the structure shown in plots of one channel against another over the whole northern hemisphere (e.g., Fig. 2) demonstrate that each channel provides more information about the surface than a simple linear relationship.

Table 1
Statistics of the 7 channels of microwave effective emissivity separated for snow and snow free surface.

		19V	19H	22V	37V	37H	85V	85H
Min	*Snow*	0.931	0.845	0.916	0.794	0.744	0.690	0.648
	Land	0.803	0.661	0.797	0.812	0.669	0.839	0.711
Max	*Snow*	1.005	0.975	1.001	0.967	0.940	0.943	0.924
	Land	0.990	0.958	0.981	0.966	0.946	0.961	0.946
Mean	*Snow*	0.977	0.921	0.962	0.900	0.851	0.813	0.880
	Land	0.935	0.875	0.928	0.923	0.872	0.919	0.877
Std	*Snow*	0.028	0.045	0.028	0.047	0.062	0.079	0.088
	Land	0.058	0.090	0.055	0.045	0.080	0.036	0.068
Mode	*Snow*	0.977	0.949	0.966	0.914	0.886	0.774	0.876
	Land	0.954	0.926	0.948	0.940	0.912	0.935	0.912

Although the scatter plot of EM19V vs. EM22V in Fig. 2 shows a quasi-linear relation with little scatter, suggesting redundant information, there is actually some structure even in this case. Although the EM37V vs. EM85V plot also shows a quasi-linear relationship, the larger scatter (compared to the EM19V vs. EM22V plot) indicates that there is additional information provided by using both channels. In the plots of EM19 vs. either EM37 or EM85 there is a little variability in EM37 and EM85 while there is a large change in EM19. These variations must be due to land surface and snow properties since the cloud contamination and atmospheric effect are removed from the data and coastal pixels were avoided (Aires et al., 2001). The complex plots for these channel combinations show that the most complete information comes from using all the channels; especially notable are the plots of EM19 vs. either EM37 or EM85.

The goal of this work is to maximize the sensitivity of microwave signal to the presence of snow. To achieve this goal we have to reduce the ambiguities. In other words, we are trying to un-mix all the contributions to the microwave signal to the maximum possible extent to isolate snow signal. We examined the frequency distributions of each twice-daily EM value (atmospheric and surface temperature effects removed) separated between snow-covered and snow-free locations using the daily snow flag from the NOAA operational product. Table 1 is the summary of the statistics for the 12 winter seasons (1993–2004) for the northern hemisphere showing the minimum, maximum, mean, standard deviation, and mode of the EM distributions for each channel for snow-covered and snow-free (called land) locations separately. Fig. 3 shows the histograms of the individual EM values for four channels, separated into snow-covered and snow-free locations (the histograms are normalized to total population of the data in percentages). The table and figure clearly show both large ranges of EM values with a concentration of values between 0.85 and 0.95. Notably, the range of both the snow-covered and snow-free effective emissivities for the lowermost frequencies is similar, with the snow-free mode value shifted to slightly lower values. The large overlap of the snow-covered and snow-free distributions shows that EM19 is not very sensitive to the presence of snow and that the effective emissivities still exhibit large variations with location. At higher frequencies (37 and 85, H polarization not shown) the

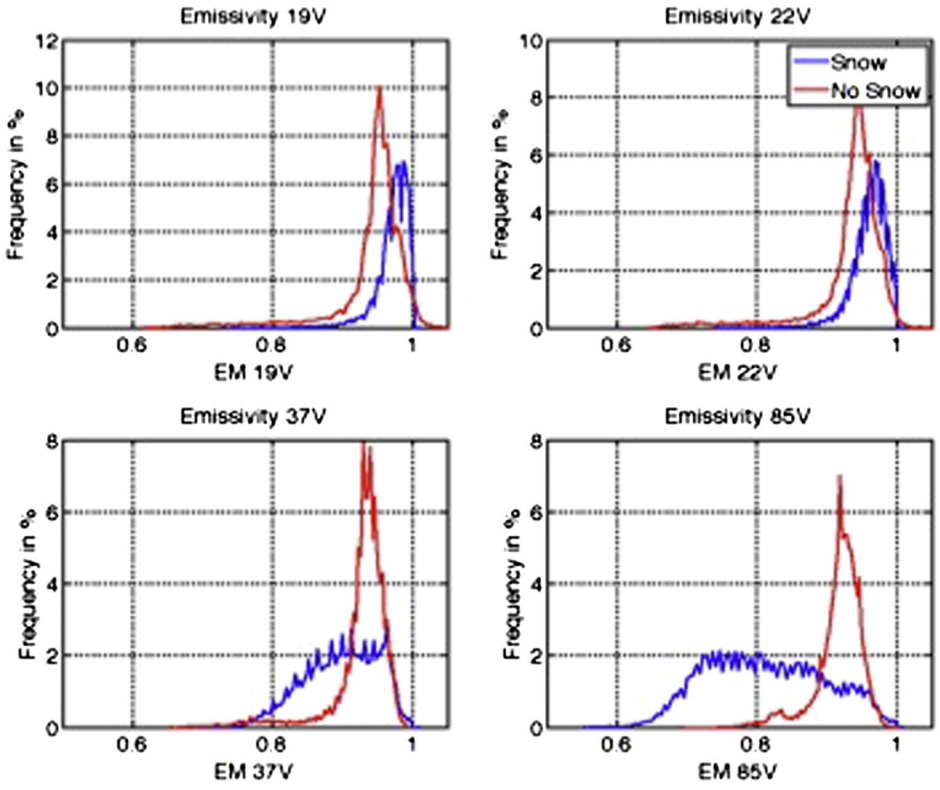

Fig. 3. Global normalized histograms of the effective emissivity for 4 channels separated for snow and snow free surface using the NOAA snow cover map.

range of snow effective emissivity values is larger than the range for snow-free locations, especially EM85, indicating a much larger sensitivity to the presence of snow. However, the overlap of the snow-covered and snow-free effective emissivities is still substantial, especially EM37, so detection of all snow-covered cases is not straightforward.

The similar distributions of EM19 and EM85 for snow-free conditions but the very different sensitivity of these two channels to the presence of snow suggest looking at effective emissivity differences to find a distinct threshold for separating the snow-covered from snow-free locations. In particular, Fig. 3 suggests that the snow-free values of EM19–37 and EM19–85 will be small, close to zero, but the values for snow-covered locations will be much larger. All possible effective emissivity differences were examined to look for the combination with the least overlap between the snow-covered and snow-free distributions. The four smallest overlap percentages from all combinations are from EM19V–37V (11.4%), EM19H–37H (11.4%), EM19V–85V (10.6%) and EM19H–85H (10.5%), where the next smallest overlap percentage is around 23%. The snow-free mean effective emissivity difference is very close to zero for these four combinations, EM19V–37V (0.003), EM19H–37H (0.005), EM19V–85V (0.002) and EM19H–85H (0.000).

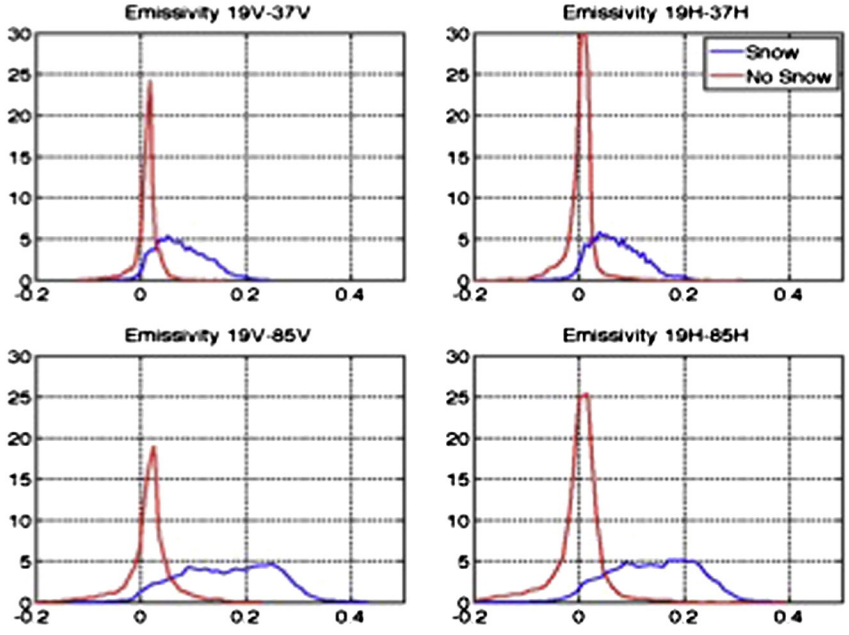

Fig. 4. Global normalized histograms of the effective emissivity for 4 combination channels separated for snow and snow free surface using the NOAA snow cover map.

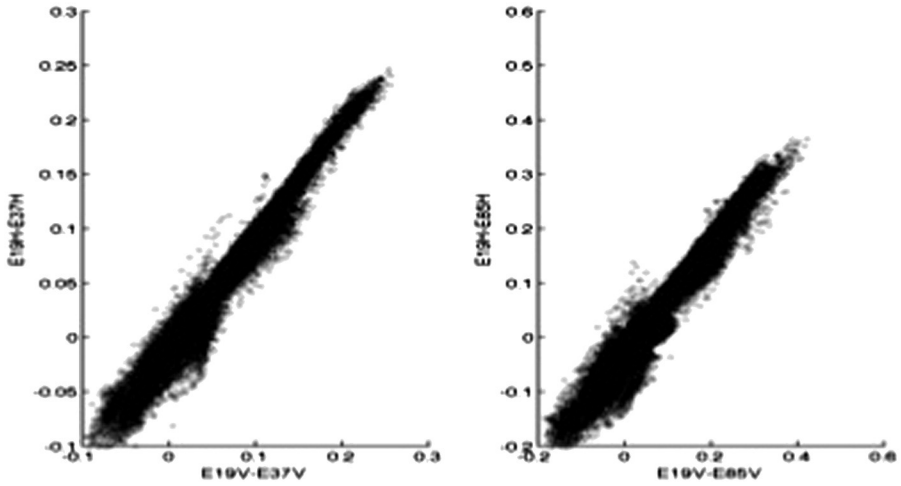

Fig. 5. Scatterplot of effective emissivity channel 19V–37V vs. 19H–37H (left) and 19V–37V vs. 19H–37H (right).

EM19V–22V and EM37V–85V also have (0.001) snow-free mean but their overlap percentages are 23% and 34% respectively. The same four channel combinations have snow-free standard deviations that are also the smallest where EM19V–37V and EM19H–37H are 0.021 *and* EM19V–85V and EM19H–85H are 0.011. Fig. 4 shows the snow-covered and snow-free effective emissivity differences for the four best combinations.

Fig. 4 shows clearly that EM19–85 provides the best separation of snow-covered from snow-free locations with only a small overlap of the two distributions. Fig. 5 shows that, from the standpoint of separating snow-covered from snow-free locations, the two polarizations are not significantly different, although the scatter about the quasi-linear relationships indicates that there is still some information to be gained using all channels. Although we continue our search for the best snow detection method by examining results from both polarizations, we will show only the V polarization results henceforth. We emphasize, however, that retrieval of snow properties should again consider all the channels to exploit the full information content.

3.2. Vegetation dependence

To understand the overlapping parts of the histograms in Fig. 4, we investigate the causes of the range of snow-free effective emissivity differences. The mean summer maps (June, July, Aug) of the effective emissivity differences, where the same snowy pixels are snow free, were examined. The statistics show that, when there is no snow on the ground, the mean summer effective emissivity difference still varies significantly with surface type and geographically within each surface type (Fig. 6) with somewhat more difference among different vegetation types for EM19–85 than for EM19–37. Although the distributions in Fig. 6 suggest that the snow-free effective emissivity differences (and effective emissivities, not shown) are associated with differences in vegetation, the large range of values for each vegetation type shows that vegetation type provides only a weak discrimination among different locations. In other words, two different locations classified as the same vegetation type can exhibit variation of effective emissivity

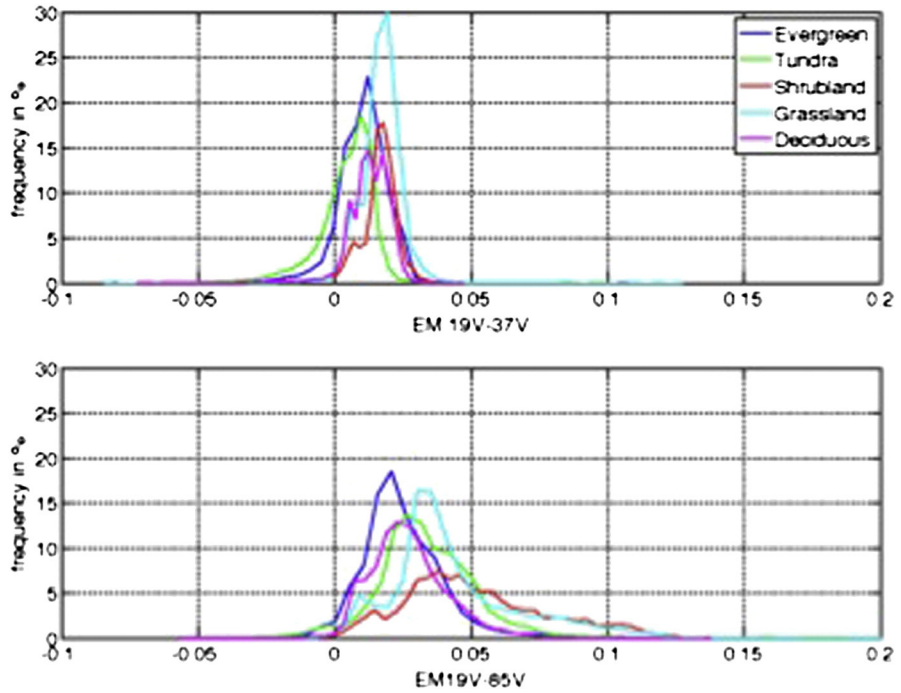

Fig. 6. Normalized histograms for 2 combination channels of effective emissivities separated for different kinds of land cover using vegetation classification over summer 2002 for snow free pixels.

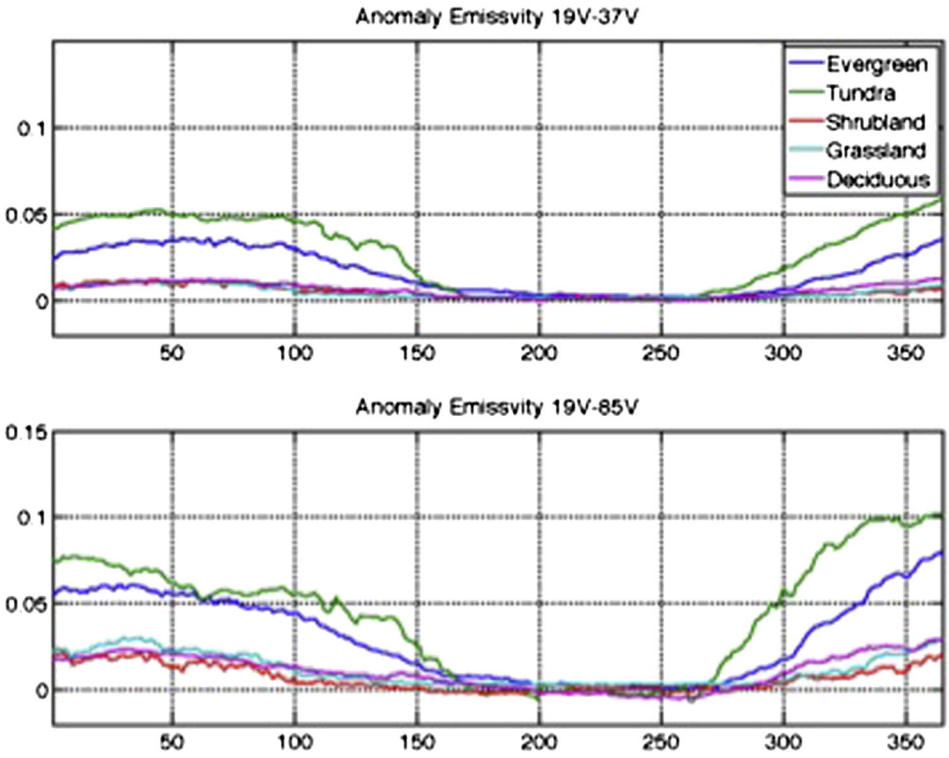

Fig. 7. Anomaly effective emissivity time series for 1 year (2002) for 2 combination channels for 5 different vegetation types.

differences (and effective emissivities) that are as large or larger than the contrast between two different vegetation types. Nevertheless, we use the vegetation classification data to separate the effective emissivity difference distributions, mostly for illustrative purposes. Although we examined global results using all nine land cover classes, we focus on the five types where there is winter snow cover: evergreen forest with 20%, deciduous forest with 22%, grassland with 19%, shrubland with 7%, and tundra with 12% of the total Northern Hemisphere land area. The sum of these 5 vegetation types covers 80% of the whole Northern hemisphere and will be counted as our total area for the rest of the paper. Fig. 6 shows the distributions of EM19–37 and EM19–85 for these locations from the summer season.

The fact that the range of effective emissivity differences within a vegetation class is as large or larger than the difference between vegetation classes suggests a different approach for reducing the geographic variations of the effective emissivities of the land surface underlying the snow cover. We calculate for each location (at 25 km intervals) the temporal anomaly of the effective emissivity differences (δEM) with respect to its summer-season mean value (Eq. 1).

$$\begin{aligned} \delta EM19{-}37 &= EM19{-}37 - [EM19{-}37] \\ \delta EM19{-}85 &= EM19{-}85 - [EM19{-}85] \end{aligned} \quad (1)$$

where [] indicates the average over the summer season at the same location.

Fig. 7 shows the annual progression of δEM19–37 and δEM19–85 averaged for each of the five vegetation types. There are three notable features in this figure. First, the variability of δEM during the summer is extremely small compared with the seasonal variations produced by snow. In other words, the background land surface values of δEM are very stable in time. Second, that the average δEM values for snow-free conditions are so small indicates that we have eliminated most of the "non-snow" variability using these quantities. Third, we note that the effects of snow are larger for δEM19–85 than for δEM19–37 as might be expected. Finally the figure shows that the effect on the δEM values is largest for the tundra and evergreen locations.

The (approximately) 10% overlap of the snow-covered and snow-free distributions of effective emissivity difference has been reduced by about a factor of 3–4 for the anomaly emissivity difference. The reduction is largest for EM19–85 as expected. By subtracting the mean summer effective emissivity difference from the daily effective emissivity differences in winter, we are taking out a constant offset approximately representing the effect on the microwave signal from the underlying land surface. Since the microwave sensitivity to the underlying surface can disappear for higher frequencies and larger snow depths (50 to 100 cm at 37 GHz depending on density and grain size (Liang, Xu, Andreadis, Josberger, & Tsang, 2008)), this approach can underestimate the snow signal for deeper snow cover. Nevertheless, variations in δEM should have only the snow signal without the geographic variations of vegetation properties. The anomaly values for snow free areas become much smaller and closer to zero (generally less than 0.05) and the snow signal becomes more distinct.

The histograms (normalized by total sample size) of δEM19–85 for all 5 vegetation types for the whole 12-year record are shown in Fig. 8 to illustrate the separation of snow-covered and snow-free signals that has been achieved. The range of snow-free values is noticeably smaller and concentrated near zero. The range of snow-covered values is shifted to larger values and a clearer separation of snow/snow free is apparent. Only about 1% of the snow-free δEM19–85 values are above 0.05. We conclude that any value of δEM19–85 above 0.05 is snow-covered, whereas values below 0.05 are still a mix of snow-covered and snow-free locations.

3.3. Temperature dependence

The overlapping snow/snow free parts of the δEM19–85 distributions for evergreen, deciduous, grassland, shrubland, and tundra represent relative fractions of about 3%, 6%, 11%, 8%, and 3%, respectively, showing that deciduous and grassland cause the most ambiguity in snow detection in the microwave. Therefore, we look for additional information that might help detect snow over these surfaces. The other quantity obtained in the retrieval of the surface effective emissivities

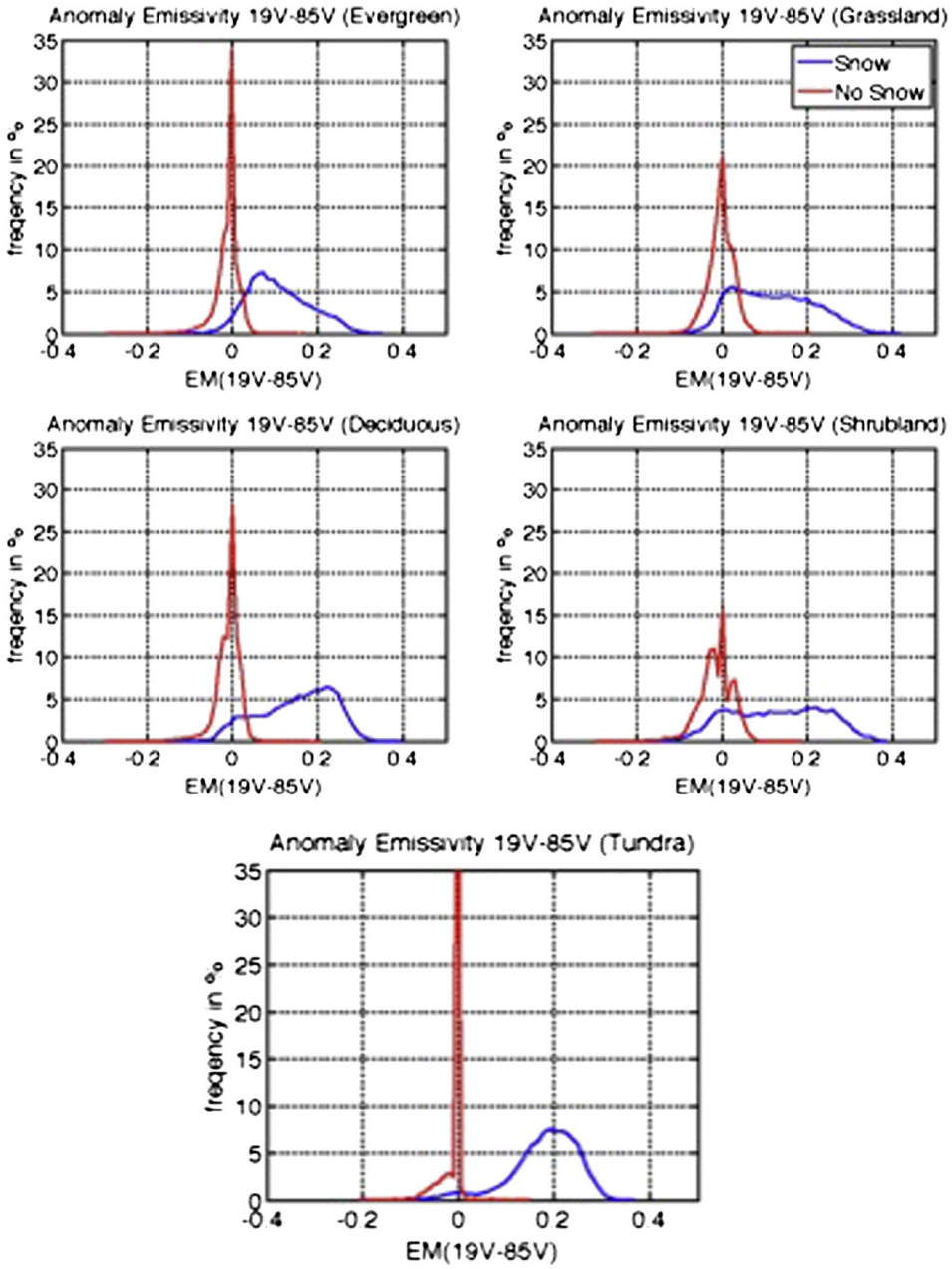

Fig. 8. Normalized histograms of anomaly effective emissivity of 19V–85V channels for 5 different vegetation types separated for snow and snow free surface using snow cover maps. (The y-axis was cut at 8% for a better visualization but their percentages are shown of the graph.)

is the corresponding skin temperature (TS): since we are using only the clear scenes, this value comes from collocated and coincident IR radiance retrievals from the ISCCP data product. In Fig. 1 for the same month of December, mean TS varies between −40 and +20. In Fig. 9 the skin temperatures are plotted vs. EM19V, EM85V, EM19–85 and δEM19–85 for the month of December. The first use of this figure is to check whether the effective emissivities are correlated with temperature, that would indicate some residual dependence or whether the skin temperature data can be used as extra information together with the effective emissivities to detect snow. The scatter plot for EM19V shows that it is not simply proportional to skin temperature, as would be the case if we did not remove all of the physical temperature variations from the brightness temperature variations. This argues that we have removed the physical temperature dependence. However, EM85V does exhibit a relationship with TS but such a relationship would be expected to be caused by the temperature dependence of snow properties. The scatterplots of the EM19–85 and δEM19–85 both show a generally negative relation with skin temperature consistent with the idea that as temperature increases, the effective emissivity difference or its anomaly decreases towards snow-free values, implying that TS might be useful for separating snow-covered and snow-free locations.

To explore this possibility, we show in Fig. 10a and b the scatter plots for deciduous and grassland for 1 day (as an example) of the values of δEM19–85 vs. TS, where the color-coding indicates how the operational NOAA product labels each location. As can be seen there are some locations with δEM19–85 < 0.05 and TS < 0 °C that are labeled as both snow-covered and snow free but this is also true for TS > 0 °C; likewise for δEM19–85 > 0.05 there are both snow-covered and snow-free locations both above and below TS = 0 °C. The figure shows one day of the data for clarity but Table 2 shows the statistics for daily data over all 12-winter seasons, showing the percentage of the snow-

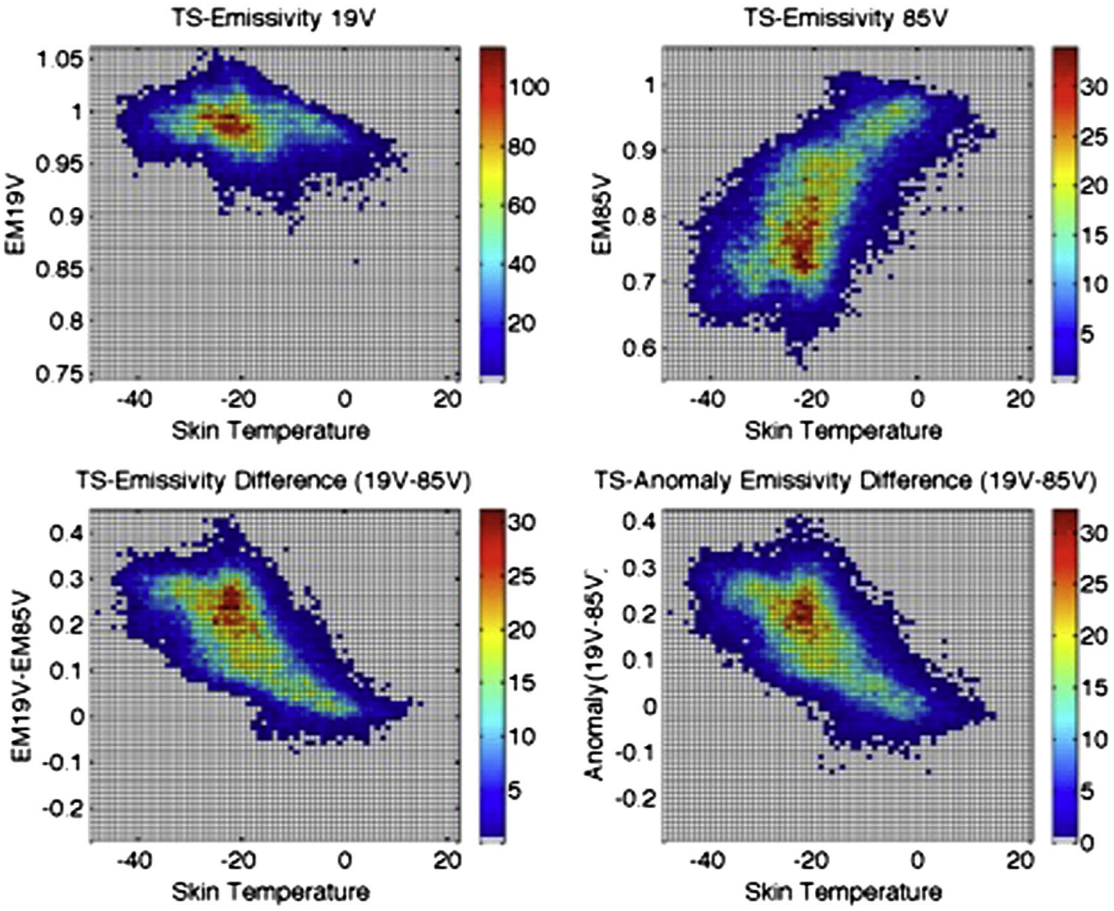

Fig. 9. Scatter plots of single frequency channels, difference frequency, and anomaly frequency difference of effective emissivity versus skin temperature where the color bar shows the percentage of distribution of the point. (For interpretation of the references to color in this figure legend, the reader is referred to the web version of this article.)

covered and snow-free pixels according to the NOAA product for each combination of δEM above and below 0.05 and TS above and below 0 °C for the 5 vegetation types. As already shown, almost all locations with δEM19–85 ≥ 0.05 are labeled as snow-covered and almost all locations with δEM19–85 < 0.05 and TS > 0 °C are labeled as snow free. The key result is that almost all locations with δEM19–85 < 0.05 but TS < 0 °C are also labeled as snow-covered. The worst disagreement according to the NOAA product is for deciduous forests, but this case is also difficult for a mostly-visible-image-based analysis.

Thus, we modify our snow detection procedure as defined by Eq. (2).

$$\begin{aligned} &\textit{If } \delta EM19{-}85 \geq 0.05 && => \text{Snow} \\ &\textit{If } \delta EM19{-}85 < 0.05 \;\&\; TS < 0 && => \text{Snow} \\ &\textit{If } \delta EM19{-}85 < 0.05 \;\&\; TS \geq 0 && => \text{No snow}. \end{aligned} \tag{2}$$

Eq. (2) is applied to the data and the results compared with the operational NOAA snow cover product. Fig. 10c and d illustrates these new results for one day over grassland and deciduous; Table 2 contains the statistics for all 12 years. The colors now indicate the following: cyan means both datasets agree that the location is snow-covered and red means both datasets agree that the location is snow-free. There are four classes of disagreement: class 1a (yellow) are locations with δEM19–85 > 0.05 and TS > 0 that we call snow-covered that are called snow-free by the NOAA product, class 1b (black) are locations with δEM19–85 > 0.05 and TS < 0 that we call snow-covered that are called snow-free by the NOAA product, class 2 (magenta) are locations where δEM19–85 < 0.05 and TS < 0 °C that we call snow-covered but the NOAA product labels as snow-free, and class 3 (green) are locations where δEM19–85 < 0.05 and TS > 0 °C that we call snow-free but the NOAA product labels as snow-covered. About 50% to 90% of the pixels for each of the vegetation types in winter have δEM19–85 above 0.05 where shrubland is the lowest (47%) and tundra is the largest (94%) and the combination of all vegetation is 63%. Around 5% to 30% have δEM19–85 below 0.05 and TS below zero and around 10% to 45% have δEM19–85 below 0.05 and TS above zero. The disagreement frequency for the combination of all vegetation types are 1% for class 1a and 1b, 3% for class 2, and 1.6% for class 3 (Table 2).

4. Evaluation of the snow detection

As discussed in the previous section and shown in Table 2 there is agreement for about 90% of all locations between the proposed algorithm and the NOAA product and about 10% disagreement. For snow detection, deciduous is the most problematic vegetation type and for the snow-free detection, shrubland is the most problematic one. Therefore, although the effect of vegetation was removed from the effective emissivity it can still disturb the signal. The uncertainty in the ISCCP temperatures at high latitudes is about ±2–3 K under clear wintertime conditions (Moncet, Liang, Lipton, Galantowicz, & Prigent, 2011; Prigent et al., 2003b), so we first test the sensitivity of the disagreements by changing the skin temperature threshold to +2 °C or −2 °C instead of zero. If the threshold is +2 °C instead of 0 °C, the snow-detection disagreement (class 2) for all vegetation increases by 3% and the snow-free detection disagreement (class 3) decreases by 1%. If the threshold is changed to −2 °C the snow-detection disagreement (class 2) for all vegetation decreases by 3% and the snow-free detection disagreement (class 3) increases by 1%. Therefore, there is about 6% change in the disagreement percentages for the snow-detection and 2% for snow-free detection when the temperature threshold is changed. In other words, about half of the disagreements could be due to the TS errors.

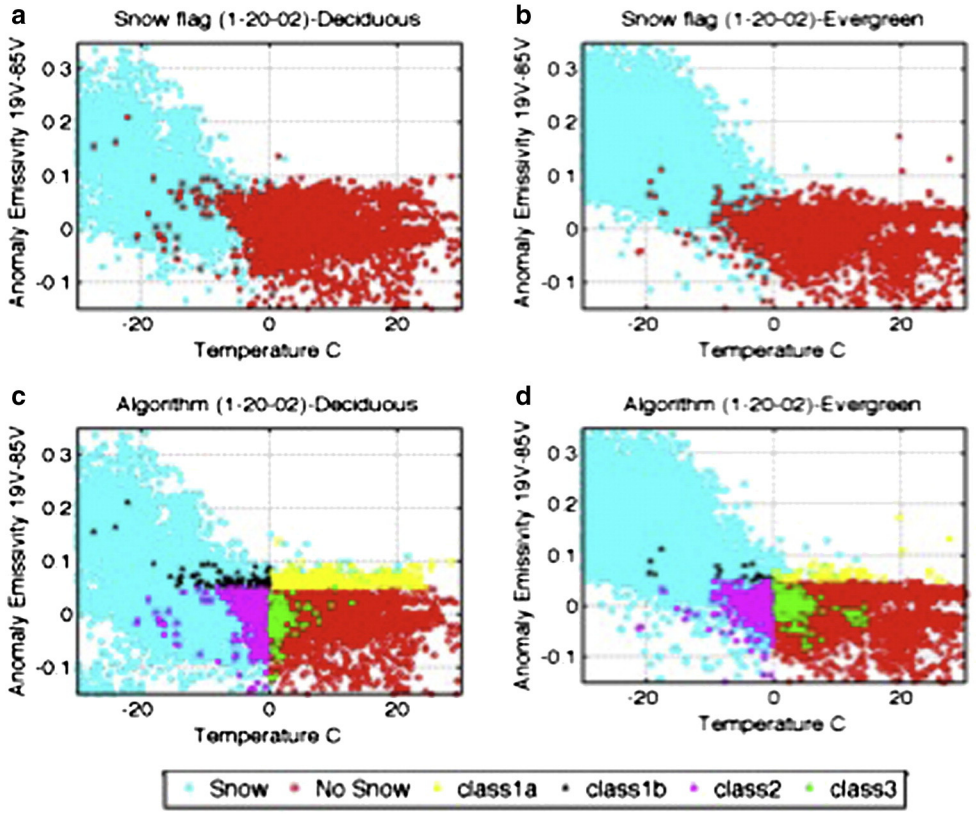

Fig. 10. Scatterplots of anomaly effective emissivity of 19V–85V vs. skin temperature for 2 different vegetation types. Top) snow (cyan) and snow free (red) separated using NOAA snow flags. Bottom) Snow (cyan) and no snow (red) separated using the proposed algorithm where classes 1a, 1b, 2, and 3 are the disagreement with NOAA snow flags. (For interpretation of the references to color in this figure legend, the reader is referred to the web version of this article.)

The behavior of the 10% of cases that disagree was studied individually for each of the four classes described in Section 3. To aid in the study of these pixels, we bring in precipitation information from GPCP. Three situations were found that explained most of the disagreement in the four classes: a) rapid melt/freeze events, b) precipitation, and c) ice cover labeled as snow. These three types of situation explain about 90% of the disagreements, that is 9% of the 10%. The pixels which did not fall into any of these situations (about 1%) are called "un-explained". We illustrate each of these situations and show what percentage of each class can be explained by these situations.

Table 3 shows the percentages for 12 years for each of the four disagreement classes and four situations. In the first column, the table shows the percentage of each of the vegetation type in the whole dataset. The second column shows the percentage of each of the classes (1a, 1b, 2, 3) for each of the vegetation types. The next four columns show the percentage of each of the disagreement classes that are associated with each of the situations (melt/freeze, precipitation, ice, un-explained). For instance, evergreen is 25% of the total data, class 1a is 41% of that 25%, and melt/freeze is 52%, precipitation is 15%, ice is 28%, and un-explained is 5% of that 41%. This means that the disagreements in class 1a for evergreen as a percentage of the total dataset are

Table 2
Percentages of δEM19–85[a] for different vegetation types showing how much data falls above .05, below .05 and below TS 0, and below 0.05 and above TS 0.

Vegetation	Flag	δEM19–85 > 0.05	δEM19–85 < 0.05 TS < 0	δEM19–85 < 0.05 TS > 0
Evergreen	*Snow*	78.35%	9.08%	0.81%
	No snow	0.82%	0.66%	10.29%
Deciduous	*Snow*	53.79%	17.37%	0.31%
	No snow	2.15%	8.04%	18.33%
Grassland	*Snow*	45.91%	30.75%	2.72%
	No snow	1.08%	3.72%	15.81%
Tundra	*Snow*	93.37%	5.67%	0.09%
	No snow	0.52%	0.14%	0.21%
Shrubland	*Snow*	24.25%	25.62%	5.48%
	No snow	0.84%	4.43%	39.39%
All vegetation	*Snow*	61.99%	17.27%	1.67%
	No snow	1.07%	3.04%	14.95%

Table 3
The percentage of each of the vegetation type in the whole dataset. Second column is the percentage of each of the classes for each of the vegetation types. The next four columns show the percentage of each of the disagreement classes that are associated with each of the situations.

Vegetation	Class	Melt/ freeze	Precipitation	Ice	Un-clarified
Evergreen	1a (41%)	66	29	0	5
25%	1b (02%)	46	20	28	6
	2 (44%)	48	14	34	4
	3 (13%)	59	33	0	8
Deciduous	1a (34%)	65	33	0	2
27%	1b (01%)	25	2	67	6
	2 (65%)	30	11	55	4
	3 (01%)	96	0	0	4
Grassland	1a (20%)	64	25	0	11
24%	1b (01%)	30	22	38	10
	2 (58%)	59	5	24	12
	3 (21%)	67	28	0	5
Shrubland	1a (10%)	83	10	0	7
15%	1b (01%)	66	9	13	12
	2 (46%)	74	12	4	10
	3 (43%)	63	26	0	11
Tundra	1a (0%)	0	0	0	0
9%	1b (42%)	74	0	23	3
	2 (58%)	12	0	88	0
	3 (0%)	0	0	0	0

5.3%, 3.2%, 2.2%, and 0.2% for melt/freeze, precipitation, ice, and un-explained, respectively.

The melt/freeze situation accounts for the largest percentage of all the four disagreement classes and all vegetation types. We examine the day-to-day variations of IR skin temperature of the pixels in each class centered on the day of disagreement. A melt event happens when TS of a pixel is below zero on one day and is suddenly above zero on the next day and a freeze event happens when TS of a pixel is above zero on one day and is suddenly below zero on the next day. This causes the snow to melt (melting does not have to be complete) or surface water to freeze suddenly; therefore the surface dielectric constant on day one will be different from that on the next day. Since the dielectric properties of liquid and frozen water at microwave frequencies are very different, the change of phase produces a substantial variation on surface effective emissivity. Therefore, even though the temporally sparse visible observations label these pixels as snow-covered or snow-free over these few-day intervals (remember that a visible-image-based snow detection obtains results only under clear conditions, which limits the time sampling to a scale of a few days), the microwave observations sense the changes (melt or freeze). More than 50% of each disagreement class is explained by rapid melt/freeze events; shrubland has the highest and tundra the lowest percentage in this situation.

The situation with the next largest percentage after melt/freeze is precipitation. We used the GPCP daily precipitation data to check if there was a precipitation event at those pixels on the specific days of disagreement. Between 5% and 30% of the pixels in each of the classes can be explained by contamination by rainfall or snowfall events. The microwave effective emissivities used in this study are obtained under the clear sky conditions as indicated by the coincident ISCCP cloud product. However, each 0.25-degree map grid cell contains only a one-pixel sample from ISCCP; this sample is a single pixel about 5 km across, so the ISCCP dataset only samples about 4% of the 0.25-degree area. Thus, it is possible on rare occasions that the low areal coverage by ISCCP and the low spatial and temporal resolution of GPCP (1°, daily) can allow for some instances of coincident clear conditions and precipitation. The GPCP data does not say if the precipitation is in form of rain or snow. If the temperature of that pixel is above about −5 °C the precipitation (about 2/3 of the precipitation error falls into this category) is most likely in the form of rain and which will change the surface dielectric constant, causing an error in the snow detection. If the temperature of that pixel is below about −5 °C the precipitation is most likely in the form of snow (about 1/3 of the precipitation error falls into this category) so the sensitivity of the higher frequency microwave to falling snow (Skofronick-Jackson, Kim, Weinman, & Chang, 2004) can produce an error in the snow detection. Evergreen and grassland have the largest percentages of this situation (about one fifth to one third of the disagreements) but this situation does not occur over tundra.

Another situation is when $\delta EM19\text{-}85 < 0.05$ and TS is very cold, below −20 °C. These pixels are called snow-covered according to Eq. (2). The NOAA snow cover product labels some of these pixels ice-covered and some of them as snow-free. Including the ice cover part of the NOAA dataset accounts for more than 50% of the pixels with very cold TS. The ice product labels Greenland (and Antarctica) as permanent ice where there could be snow on the ice. However, as the summertime mean EM difference, is actually representative of ice cover, the values of δEM19–85 do not indicate snow-cover. Tundra has the largest percentages in this situation.

The un-explained situation is where none of the above explanations applies. This situation occurs about 5% to 12% for each disagreement class with Shrubland and Grassland having the highest percentages (equalized to 1% of the total dataset). Some of these cases can be explained by the mismatch of temporal and spatial resolutions as discussed in Section 2, where it was shown that about 2–4% of the disagreements can be explained by these mismatches and TS errors (Moncet et al., 2011)

Of the 10% of cases where there was apparent disagreement about the presence or absence of snow, the rapid melt/freeze events explained the largest percentage (more than half) of these and the un-explained situations accounted for less than 10% (1% of the total data). Deciduous and grassland have the largest disagreement for snow detection (classes 1a, 1b, and 2) and shrubland has the largest disagreement for snow-free detection (class 3), mostly due to rapid melt/freeze events. Class 1b (where $\delta EM19\text{–}85 > 0.05$ and $TS < 0$) has a very small percentage (less than 1% of the total data) compared to the other classes and can be neglected. There are number of studies on melt/freeze of snow during melting seasons using visible, passive and active microwave data (Foster et al., 2011; Royer, Goita, Kohn, & De Seve, 2010). There is about 90% agreement between the snow detection algorithm (Eq. 2) and the NOAA product. To confirm this agreement, our snow detection results are next compared with other available snow cover datasets.

5. Comparisons

The results of our snow detection procedure were compared with three different datasets: the daily NOAA IMS snow cover (a mixed visible and microwave based product), the Canadian Meteorological Center (CMC) snow depth (a completely satellite-independent product), MODIS snow cover (a visible-NIR based product), and another microwave product near-real time ice and snow extent (NISE) (a microwave brightness temperature product). The accuracy of these maps is not known either but the techniques used to map snow cover in the various maps are very different. Each of these snow cover maps was also compared to each other.

5.1. IMS

The IMS product is manually created by a satellite analyst looking at all available satellite imagery, several automated snow mapping algorithms, and other ancillary data. For snow extent, they rely primarily on visible band satellite imagery. The analyst begins with a previous day's map as a first guess and changes it only if there is data available for that day. Thus the effective time resolution is a few to many days. We compared the daily IMS snow product with our snow detection algorithm snow product for five available matching years (2000–2004). As it is shown in Table 4 about 51% of the snow data are above the anomaly 0.05 and 15% is below 0.05 with skin temperature below zero, which says 66% of the data agree for snow and about 16% below anomaly 0.05 with skin temperature above zero says the data agree for no snow. There is about 17% disagreement, where some of it can be explained by the filling of the data with the pervious available observation.

5.2. CMC

Snow depth data from CMC were compared with our results showing about 74% snow agreement, 11% no-snow agreement, and 14%

Table 4
Comparison of the anomaly effective emissivity snow test with IMS, CMC, and MODIS, NISE.

	Flag	δEM19–85 > 0.05	δEM1985 < 0.05 TS < 0	δEM1985 < 0.05 TS > 0
(*IMS*)	*Snow*	51.49	14.67	4.26
	No snow	4.78	08.93	15.84
CMC	*Snow*	51.60	22.34	5.77
	No snow	4.05	04.99	11.22
MODIS	*Snow*	48.07	10.09	1.92
	No snow	0.52	05.90	33.47
NISE	*Snow*	32.76	03.93	3.10
	No snow	06.07	12.24	41.8

Table 5
Comparison of MODIS snow fraction in 25 km resolution with the snow detection algorithm for 5 years (2000–2004). Column 1 shows MODIS snow coverage, column 2 shows the percentage of the pixels that fall in that category for the whole globe and the whole 5 - years, and column 4 shows the percentage of the pixels that agree/disagree with MODIS using our snow detection algorithm.

MODIS snow fraction	Pixel percentage	Snow detection algorithm	
0%	59.04	*Snow*	15.14
		No snow	84.92
1–25%	3.56	*Snow*	59.66
		No snow	40.34
25–50%	2.37	*Snow*	74.76
		No snow	25.24
50–75%	2.48	*Snow*	79.33
		No snow	20.67
75–99%	2.99	*Snow*	81.76
		No snow	18.24
100%	29.55	*Snow*	98.77
		No snow	1.23

disagreement. The disagreement may be increased by the fact that the CMC data are station (point) data, whereas the satellite data has a 25 km footprint (Table 4). The IMS and the CMC are in good agreement with each other at about 91%.

5.3. MODIS

The MODIS snow product has a lot of missing data on a given date because pixels during night and cloudy sky conditions have no snow report. More than 50% of the MODIS data in the northern hemisphere during the snow season fall into the night and/or cloudy category each day, where snow detection is not possible. Only the available pixels with each other at each day for 5 years (2000–2004) were compared in such a way that all the 500 m pixels of MODIS were averaged in a 25 km pixel (matched with the passive microwave) and if the snow percentage was more zero the pixel was called snow. This comparison showed 58% of the snow agrees, 33.47% of the no snow agrees, and 8% disagreed (Table 4). Some of the disagreements can be due to the spatial resolution differences. Since MODIS has much higher resolution than the microwave and it reports snow cover percentage for each pixel, another comparison was done in order to check that when the MODIS snow coverage is less 100% what would the snow detection algorithm call the pixel. Looking at the 500 m resolution MODIS pixels it was found that only 6% of the snow-covered pixels have values between 1 and 99% and when the 500 m MODIS pixels are averaged to 25 km pixels this percentage only increases to 11%. When the MODIS snow coverage is 100% the snow agreement with our snow algorithm is 98%, and as the snow coverage decreases the agreement decays down to 60% for snow coverage below 25% (Table 5). From these statistics it can be said that first, averaging the 500 pixels to 25 km only increases the partial snow coverage by 5%. Second, the pixels with less than 25% snow coverage are the largest group, which are still very rare situations. Third, of this 11% of the pixels with partial snow coverage our snow algorithm detects snow pixels between 60 and 80% of the time. Comparing the MODIS snow cover with the CMC and IMS data using only available pixels of the MODIS, there is about 36% of snow agreement and 53% of no snow agreement. The remaining 10%, which disagrees, again can be due, in part, to the different spatial resolutions of the datasets.

5.4. NISE

The NISE data were compared with our results showing about 36% snow agreement and 42% no-snow agreement. There is 18% disagreement with the snow detection where 12% of it falls into the condition of $\delta EM19–85 < 0.05$ and $TS < 0$ which will be called snow with our detection but are called no-snow with the NISE products. Most of the disagreement is with the TS in the detection and about half of this 12% is due to the melt/freeze transition. This data is derived from SSM/I microwave using an algorithm (Armstrong & Brodzik, 2001) that uses the brightness temperature difference of two channels (19H–37H). Their study demonstrates that their algorithm underestimates snow extent in the presence of shallow snow; however it tends to overestimate snow extent (both wet and dry) in various locations (Nolin et al., 1998). Since we are using 85 GHz in our algorithm, which can see shallow snow better. Comparing NISE and MODIS there is 83% agreement

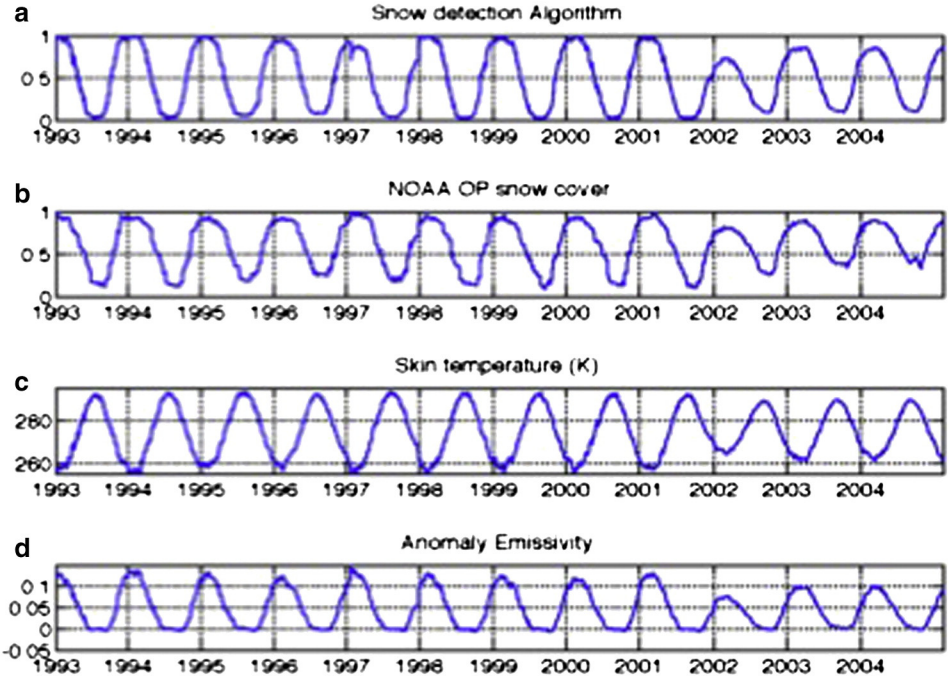

Fig. 11. Time series of amount of snow cover with snow detection algorithm, NOAA snow cover product, TS, and δEM19–85. The snow covers are normalized to the maximum values (a & b).

between them. MODIS is the visible-infrared based snow product that agreed best (92%) with our snow algorithm, which shows we have a more sensitive microwave-based algorithm than NISE.

6. Interannual Variability of snow-cover

One motivation for producing an accurate snow detection dataset, besides using it to study snowpack properties and behavior, is to be able to study the slow interannual variations of snow cover that are not only indicators of climate change but also an important positive feedback on global warming as reduced snow cover leads to increased solar heating. To understand the atmospheric and surface processes involved requires resolving the time variations at scales commensurate with weather events. Such studies will have to extend the daily (or even twice-daily) microwave snow cover detection to retrievals of the physical properties of the snow and combine these results with other data products quantifying weather events. Here, we look at the time series of the amount of the snow over the Northern Hemisphere for the 12-year record (1993–2004) produced by our snow detection algorithm to obtain a preliminary idea of the magnitude of interannual variability (Fig. 11a).

The time series in Fig. 11a shows the number of snow-covered pixels for each day divided by all the pixels for the five vegetation types in the Northern Hemisphere, normalized by the maximum value in the record. There are no changes from 1993 until the winter of 2001–2002 when there is a 10% decrease in the maximum snow cover extent as well as an increase in the summer 2002 minimum extent. Over the next few years, the maximum extent slowly increases towards its prior values but the summertime minimum extent remains the same. Fig. 11b shows the snow cover extent from the NOAA operational product, which exhibits the same decrease in the maximum extent in the winter of 2001–2002 and the same increase in the 2002 summertime minimum extent. Although the NOAA product shows the increase in the wintertime maximum extent in subsequent years, it also shows a significant increase in the minimum extent. These changes in snow cover extent may be consistent with the generally warmer average wintertime temperatures in 2001–2002 and the cooler 2002 summertime temperatures shown in Fig. 11c. In the following years, both the wintertime and summertime temperatures change back towards their previous values. Fig. 11d shows the average values of δEM19–85; the variations are consistent with a decrease of snow extent as they should be.

The timing of this apparent change in snow cover and temperatures is unfortunate, since there is a known increase of the ISCCP global monthly mean TS values by a little less than 3 K between September and October 2001 that is produced by a change in the atmospheric temperature–humidity product (TIROS Operational Vertical Sounder, TOVS) used by ISCCP to retrieve surface skin temperatures (Zhang et al., 2004). Since the effect on surface temperature depends on the changed atmospheric absorption of infrared emission from the surface as well as atmospheric emission, both of which depend on the water vapor abundance, the magnitude of the change in high latitude wintertime TS values is weaker than the global mean change. To investigate whether this affects our results, we first examined maps of monthly temperature differences (we are looking for a bias) between September and October in 2000, 2001 and 2002. We find differences in TS < 5 K in lower latitudes but much smaller changes at higher latitudes: the decrease of TS from September to October (difference of monthly averages over the area for the five vegetation types) is about 8 K in 2000 and 7 K in 2002, when there is no systematic change of the TOVS product between months. However, in 2001, this change is only a little over 5 K, suggesting that the TOVS change may have reduced the seasonal decline of TS by up to 3 K — the change of TS in wintertime will be smaller still.

A spurious change in TS can affect our snow detection in two ways. First, since we use a TS test as part of the detection algorithm, any shift of TS could induce a bias of snow cover. The threshold sensitivity test we described earlier in Section 4 shows that snow extent would change by only about 2–3% for a 2 K change in TS. However, Fig. 12 shows the fraction of the total snow cover detected by the effective emissivity-only and the temperature thresholds (Eq. 2), demonstrating not only that most of the snow detected by the temperature-independent threshold on δEM19–85 but also that all of the decrease in snow cover extent comes from the effective emissivity part of the algorithm. So the TS change from ISCCP is not large enough to explain the 10% decrease in snow cover extent. The second way that TS can affect our results is in the retrieval of the microwave effective emissivities. However, the decrease in δEM19–85 comes entirely from the EM85 (not shown). The fact that EM85 changes, but EM19 does not, is inconsistent with a temperature-induced error in the microwave retrieval which requires the same physical temperature for all microwave channels. Thus,

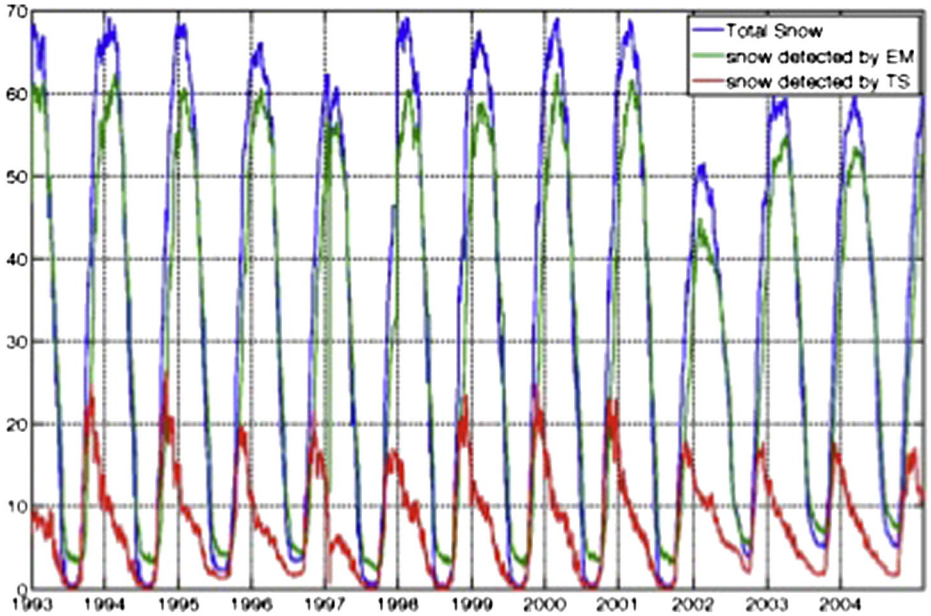

Fig. 12. Time series of percentage of snow cover over land with snow detection algorithm, for total snow, snow detected by effective emissivity, snow detected by TS.

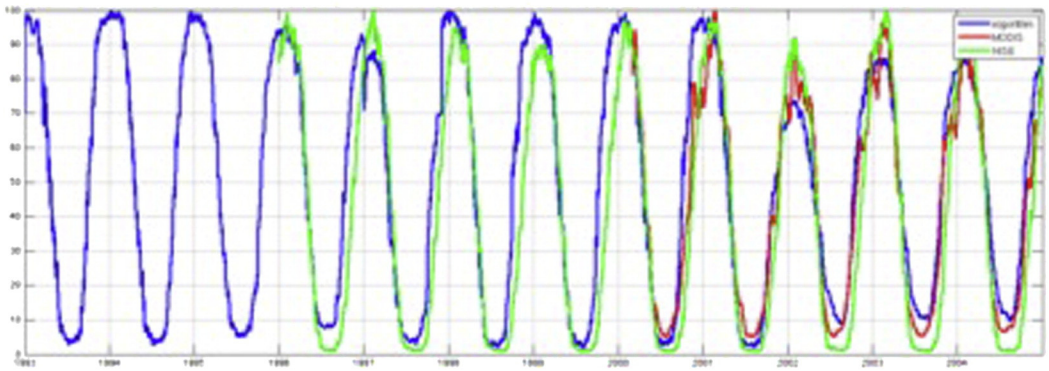

Fig. 13. Time series of the amount of the snow cover for the snow detection algorithm for the 12-year record (1993–2004), NISE for 9-year (1996–2004), and MODIS for 5-year (2000–2004).

if a change in EM is to be associated with a change in TS, all channels should exhibit similar changes. Any residual effect of the biased TS value input to the retrieval from ISCCP is further mitigated by using EM differences in our detection algorithm. Thus, we conclude that the sudden change of the ISCCP TS values between September and October 2001 cannot explain the decreased snow cover extent that we obtain in the following winter of 2001–2002 relative to previous winters. Moreover, the interannual evolution of the ISCCP TS values after 2001 shows no significant trends to explain the subsequent slow increase of wintertime snow cover extent. We also note that the baseline NOAA operational snow cover product shows the same decrease in snow cover but by about 12% (Fig. 11b), the MODIS snow cover product shows a similar decrease but by about 7%, and the NISE data shows about 4% decrease (Fig. 13). The other two snow products, IMS and CMC, do not exhibit any changes (not shown). More investigation of the possible variations of snow cover extent is warranted to verify this result.

7. Conclusions

Passive microwave has advantages over other satellite measurements for snow detection because it provides results day and night and under most weather conditions. The effective emissivity product used in this analysis has the advantage of having the contributions of the atmosphere, including clouds and water vapor, removed and the physical temperature variations separated from the effective emissivity variations. Although this particular dataset is produced under clear sky (cloudy pixels are removed) which provides more sensitivity to ground effects, it should work when there is cloud if it is not precipitating (Aires et al., 2001).

By employing a difference of effective emissivities at low and high frequencies and determining the time-anomaly of this difference for each location, we also removed the constant effects of land surface vegetation properties, leaving only the snow signal (for deep snow layers, this procedure may underestimate the snow signal). As a test of the isolation of snow signature from the microwave signal we evaluated an algorithm to detect snow with that signal. Our snow detection results agreed about 78% with another microwave snow detection (NISE) and more than 80% of the time, with three other snow datasets (IMS, MODIS, CMC) because the IMS and MODIS depend on visible, and CMC is independent of satellite measurements.

Most of the 10% disagreements between the proposed algorithm and NOAA snow cover product can be explained by rapid melt–freeze–refreeze events, contamination by coincident precipitation mislabeled frozen ground, and spatial/temporal mismatches. The remaining unexplained cases represent only about 1% of the dataset. These disagreements point to the need for a high time resolution product that is not limited by cloud cover or solar illumination, especially to detect the rapid melt/freeze events. Also, if precipitation effects were accounted for then such a product would capture changes in the surface following snowfall (or rainfall) events. The cases of bare ice cover or snow cover on permanent ice require more careful study to determine whether the microwave can detect the changes.

A snow cover time series (12-year) was examined. The interannual variability of the snow characteristics appears to be very small but there appear to have been notable changes in the early part of this decade, a result also found in two other snow cover products. The artifact in the ISCCP TS values may have exaggerated the magnitude of this change in our results but cannot explain the whole change that we find.

Our algorithm which produced a more sensitive microwave detection of snow has also isolated the snow part of the signal (approximately) which can now be used to characterize the physical snowpack properties such as snow depth, snow density, snow grain size, and snow water equivalent. These products; 1) the snow cover product, daily snow-cover variability which shows the increase/decrease of snow cover for each day, 2) an anomaly effective emissivity difference that indicates changes in snow properties each day, and 3) the skin temperature associated with each of these pixels can all be used as inputs to future snowpack retrievals.

Acknowledgments

This work was supported by the National Oceanic and Atmospheric Administration – Cooperative Remote Sensing Science and Technology Center (NOAA-CREST) under grant number NA06OAR4810162. The authors would like to thank Cindy Pearl for providing us with technical support and fruitful discussions. The authors also would like to acknowledge Dr. Reza Khanbilvardi the director of NOAA-CREST. Comments and suggestions from the anonymous reviewers were extremely valuable in creating the final version of this manuscript.

References

Adler, R. F., Huffman, G. J., Chang, A., Ferraro, R., Xie, P. P., Janowiak, J., et al. (2003). The version-2 global precipitation climatology project (GPCP) monthly precipitation analysis (1979–present). *Journal of Hydrometeorology*, *4*(6), 1147–1167.

Aires, F., Prigent, C., Rossow, W. B., & Rothstein, M. (2001). A new neural network approach including first guess for retrieval of atmospheric water vapor, cloud liquid water path, surface temperature, and emissivities over land from satellite microwave observations. *Journal of Geophysical Research-Atmospheres*, *106*(D14), 14887–14907.

Armstrong, R. L., & Brodzik, M. J. (2001). Recent Northern Hemisphere snow extent: A comparison of data derived from visible and microwave satellite sensors. *Geophysical Research Letters*, *28*(19), 3673–3676.

Armstrong, R. L., & Brodzik, M. J. (2002). Hemispheric-scale comparison and evaluation of passive-microwave snow algorithms. *Annals of Glaciology*, *34*, 38–44 (34).

Brown, R. D., & Brasnett, B. (2010). *Updated annually. Canadian Meteorological Centre (CMC) Daily Snow Depth Analysis Data.* (edited). Boulder, Colorado USA: National Snow and Ice Data Center.

Chang, A. T. C., Foster, J. L., & Hall, D. K. (1987). Nimbus-7 SMMR derived global snow cover parameters. *Annals of Glaciology*, *9*, 39–44.

Dewey, K. F., & Heim, R. (1982). A digital archive of Northern Hemisphere snow cover, November 1966 through December 1980. *Bulletin of the American Meteorological Society*, *63*(10), 1132–1141.

Dietz, A. J., Kuenzer, C., Gessner, U., & Dech, S. (2012). Remote sensing of snow — A review of available methods. *International Journal of Remote Sensing*, *33*(13), 4094–4134.

Foster, J., Liston, G., Koster, R., Essery, R., Behr, H., Dumenil, L., et al. (1996). Snow cover and snow mass intercomparisons of general circulation models and remotely sensed datasets. *Journal of Climate*, *9*(2), 409–426.

Foster, J. L., Hall, D. K., Eylander, J. B., Riggs, G. A., Nghiem, S. V., Tedesco, M., et al. (2011). A blended global snow product using visible, passive microwave and scatterometer satellite data. *International Journal of Remote Sensing*, *32*(5), 1371–1395.

Gentemann, C. L., Wentz, F. J., Brewer, M., Hilburn, K., & Smith, D. (2010). Passive microwave remote sensing of the ocean: An overview, in Oceanography from Space, revisited (2010). In V. Barale, J. Gower, & L. Alberotanza (Eds.), Heidelberg: Springer,13–33.

Grody, N. C., & Basist, A. N. (1996). Global identification of snowcover using SSM/I measurements. *IEEE Transactions on Geoscience and Remote Sensing*, *34*, 237–249.

Hall, D., & Salomonson, V. (2006). *MODIS/Aqua Snow Cover Daily L3 Global 500 m Grid, Version 5. Version 5. [Fractional Snow Cover].* (edited). Boulder, Colorado USA: National Snow and Ice Data Center.

Hall, D. K., Sturm, M., Benson, C. S., Chang, A. T. C., Foster, J. L., Garbeil, H., et al. (1991). Passive microwave remote and in situ measurements of arctic and subarctic snow covers in Alaska. *Remote Sensing of Environment*, *38*, 161–172.

Hollinger, J. P., Lo, R., Poe, G., Savage, R., & Pierce, J. (1987). *Special sensor microwave/imager user's guide.* Washington DC: Nav. Res. Lab.

Huffman, G. J., Adler, R. F., Arkin, P., Chang, A., Ferraro, R., Gruber, A., et al. (1997). The Global Precipitation Climatology Project (GPCP) combined precipitation dataset. *Bulletin of the American Meteorological Society*, *78*(1), 5–20.

Kalnay, E., Kanamitsu, M., Kistler, R., Collins, W., Deaven, D., Gandin, L., et al. (1996). The NCEP/NCAR 40-year reanalysis project. *Bulletin of the American Meteorological Society*, *77*(3), 437–471.

Kelly, R. E. J., & Chang, A. T. C. (2003). Development of a passive microwave global snow depth retrieval algorithm for Special Sensor Microwave Imager (SSM/I) and Advanced Microwave Scanning Radiometer-EOS (AMSR-E) data. *Radio Science*, *38*(4).

Kunzi, K. F., Patil, S., & Rott, H. (1982). Snow-cover parameters retrieved from Nimbus-7 Scanning Multichannel Microwave Radiometer (Smmr) data. *IEEE Transactions on Geoscience and Remote Sensing*, *20*(4), 452–467.

Liang, D., Xu, X. L., Andreadis, K. M., Josberger, E. G., & Tsang, L. (2008). The effects of layers in dry snow on its passive microwave emissions using dense media radiative transfer theory based on the quasicrystalline approximation (QCA/DMRT). *IEEE Transactions on Geoscience and Remote Sensing*, *46*(11), 3663–3671.

Lin, B., & Rossow, W. B. (1994). Observations of cloud liquid water path over oceans — optical and microwave remote-sensing methods. *Journal of Geophysical Research-Atmospheres*, *99*(D10), 20907–20927.

Matthews, E. (1983). Global vegetation and land-use — new high-resolution data-bases for climate studies. *Journal of Climate and Applied Meteorology*, *22*(3), 474–487.

Moncet, J. L., Liang, P., Lipton, A. E., Galantowicz, J. F., & Prigent, C. (2011). Discrepancies between MODIS and ISCCP land surface temperature products analyzed with microwave measurements. *Journal of Geophysical Research-Atmospheres*, *116*.

NOAA/NESDIS/OSDPD/SSD (2004). *IMS Daily Northern Hemisphere Snow and Ice Analysis at 4 km and 24 km resolution [snow cover].* (edited by). C. U. Boulder: National Snow and Ice Data Center.

Nolin, A., Armstrong, R. L., & Maslanik, J. (1998). *Near-Real-Time SSM/I-SSMIS EASE-Grid Daily Global Ice Concentration and Snow Extent. Version 4.* (edited). Boulder, Colorado USA: NASA DAAC at the National Snow and Ice Data Center.

Prigent, C., Aires, F., & Rossow, W. B. (2003a). Land surface skin temperatures from a combined analysis of microwave and infrared satellite observations for an all-weather evaluation of the differences between air and skin temperatures. *Journal of Geophysical Research-Atmospheres*, *108*(D10), 4310–4321.

Prigent, C., Aires, F., & Rossow, W. B. (2003b). Retrieval of surface and atmospheric geophysical variables over snow-covered land from combined microwave and infrared satellite observations. *Journal of Applied Meteorology*, *42*(3), 368–380.

Prigent, C., Aires, F., Rossow, W., & Matthews, E. (2001). Joint characterization of vegetation by satellite observations from visible to microwave wavelengths: A sensitivity analysis. *Journal of Geophysical Research-Atmospheres*, *106*(D18), 20665–20685.

Prigent, C., Rossow, W. B., & Matthews, E. (1997). Microwave land surface emissivities estimated from SSM/I observations. *Journal of Geophysical Research-Atmospheres*, *102*(D18), 21867–21890.

Robinson, D. A., Dewey, K. F., & Heim, R. R. (1993). Global snow cover monitoring — an update. *Bulletin of the American Meteorological Society*, *74*(9), 1689–1696.

Rossow, W. B., & Garder, L. C. (1993). Validation of ISCCP cloud detections. *Journal of Climate*, *6*(12), 2370–2393.

Rossow, W. B., & Schiffer, R. A. (1999). Advances in understanding clouds from ISCCP. *Bulletin of the American Meteorological Society*, *80*(11), 2261–2287.

Royer, A., Goita, K., Kohn, J., & De Seve, D. (2010). Monitoring dry, wet, and no-snow conditions from microwave satellite observations. *IEEE Transactions on Geoscience and Remote Sensing*, *7*(4), 670–674.

Skofronick-Jackson, G. M., Kim, M. J., Weinman, J. A., & Chang, D. E. (2004). A physical model to determine snowfall over land by microwave radiometry. *IEEE Transactions on Geoscience and Remote Sensing*, *42*(5), 1047–1058.

Wigneron, J. P., Chanzy, A., de Rosnay, P., Rudiger, C., & Calvet, J. C. (2008). Estimating the effective soil temperature at L-band as a function of soil properties. *IEEE Transactions on Geoscience and Remote Sensing*, *46*(3), 797–807.

Zhang, Y., Rossow, W. B., Lacis, A. A., Oinas, V., & Mishchenko, M. I. (2004). Calculation of radiative fluxes from the surface to top of atmosphere based on ISCCP and other global data sets: Refinements of the radiative transfer model and the input data. *Journal of Geophysical Research*, *109*.